State-to-state photodissociation of carbonyl sulfide ($\nu_2=0,1|J\ell M$). II. The effect of initial bending on coherence of S($^1D_2$) polarization

Alrik J. van den Brom
Laser Center and Department of Chemistry, Vrije Universiteit, de Boelelaan 1083, 1081 HV Amsterdam, The Netherlands

T. Peter Rakitzis
Department of Physics, University of Crete, Heraklion 71110, Greece and Institute of Electronic Structure and Laser of the Foundation for Research and Technology-Hellas (IESL-FORTH), P.O. Box 1527, 71110 Heraklion, Greece

Maurice H. M. Janssen[a)]
Laser Center and Department of Chemistry, Vrije Universiteit, de Boelelaan 1083, 1081 HV Amsterdam, The Netherlands

(Received 2 August 2005; accepted 29 August 2005; published online 26 October 2005)

Photodissociation studies using ion imaging are reported, measuring the coherence of the polarization of the S($^1D_2$) fragment from the photolysis of single-quantum state-selected carbonyl sulfide (OCS) at 223 and 230 nm. A hexapole state-selector focuses a molecular beam of OCS parent molecules in the ground state ($\nu_2=0|JM=10$) or in the first excited bending state ($\nu_2=1|J\ell M=111$). At 230 nm photolysis the Im[$\mathbf{a}_1^{(1)}(\parallel,\perp)$] moment for the fast S($^1D_2$) channel increases by about 50% when the initial OCS parent state changes from the vibrationless ground state to the first excited bending state. No dependence on the initial bending state is found for photolysis at 223 nm. We observe separate rings in the slow channel of the velocity distribution of S($^1D_2$) correlating to single CO(J) rotational states. The additional available energy for photolysis at 223 nm is found to be channeled mostly into the CO(J) rotational motion. An improved value for the OC–S bond energy $D_0=4.292$ eV is reported. © *2005 American Institute of Physics*. [DOI: 10.1063/1.2076647]

I. INTRODUCTION

The outcome of a photodissociation process is determined by the shape of the potential-energy surface sampled during the photon excitation and the subsequent dissociation of the fragments. The initial quantum state of the parent molecule and the energy and polarization of the absorbed photon determine which part of the potential is sampled during the excitation. The subsequent pathway that the system follows on the potential-energy surfaces is eventually reflected in the electronic states and the translational, vibrational, and rotational motion of the photofragments. Not only the population of quantum states but also the directional properties of the electronic and rotational angular momentum of the photofragments reflect information on how the potential surfaces are sampled. The polarization of the angular momentum provides a profound insight into the nature of photochemical processes.

Based on a spherical tensor formalism derived by Fano and Macek,[1] as well as by Greene and Zare,[2] Kummel *et al.*[3,4] showed how the polarization of the angular momentum can be expressed as an expansion into modified spherical harmonics $C_q^k(\theta,\varphi)=(4\pi/2k+1)^{1/2}Y_{kq}(\theta,\varphi)$, where θ and φ are the photofragment polar angles in the molecular frame. The various $|q|=0,1,2,\ldots$ terms contributing to the total polarization are ramifications of physical processes that occur during the dissociation of the molecule.[5–9] Rakitzis and Zare[7] showed how the expansion into modified spherical harmonics can be separated into parallel ($\parallel$), perpendicular ($\perp$), and mixed ($\parallel$, $\perp$) types of contributions of the transition dipole moment between the molecular ground state and the dissociating excited states, thereby expressing the full quantum-mechanical treatment of the photofragment polarization of Siebbeles *et al.*[5] in terms of the molecular-frame $\mathbf{a}_q^{(k)}(p)$ formalism. This separation yields a complete description of the photofragment angular momentum polarization in the photofragment frame in terms of $\mathbf{a}_q^{(k)}(p)$ [$p=\parallel$, $\perp$ or ($\parallel$, $\perp$)] coefficients for the modified spherical harmonic expansion of the polarization. An alternative description was developed by Bracker *et al.*[6] The molecular-frame parameters that have been of great interest recently are the $\mathbf{a}_1^{(k)}(\parallel,\perp)$ parameters.[10–15] They reflect information on photofragment orientation arising from the interference of dissociative states of different symmetries or the breakdown of the axial recoil approximation.

In this paper we report the measurement of the atomic polarization of S($^1D_2$) from the photodissociation of quantum state-selected carbonyl sulfide (OCS). Carbonyl sulfide, upon excitation to the first absorption band around 220 nm, dissociates into S(95% $^1D_2$, 5% $^3P_2$) and CO($X\,^1\Sigma^+$).[16] The CO photofragment is released in the electronic and vibrational ground states, but with a considerable rotational exci-

[a)]Author to whom correspondence should be addressed. Electronic mail: mhmj@chem.vu.nl

tation. The CO(J) rotational distribution, and hence the kinetic energy release (KER), shows a bimodal structure.[17–22] The electronic ground state of OCS is linear and the excited states accessed around 220–230 nm are bent, so OCS serves as an ideal triatomic benchmark system for studying the effect of bending motion on photodissociation dynamics. Upon bending, the degenerate OCS($1\,^1\Delta$) excited state splits into the $2\,^1A'$ and the $2\,^1A''$ states, and the $1\,^1\Sigma^-$, which is energetically close to the $1\,^1\Delta$ state when the molecule is linear, becomes the $1\,^1A''$ state. The electronic ground state is linear and has a $1\,^1A'$ symmetry. It increases strongly in energy for a bent geometry. Calculations by Suzuki *et al.*[19] suggest that after excitation to the $2\,^1A'$ state, a nonadiabatic interaction between the $1\,^1A'$ ground state and the $2\,^1A'$ excited state causes a splitting of the initial wave packet. This splitting was suggested as the origin of the bimodal KER and CO rotational distribution. In the wavelength range of 223–230 nm, only the $1\,^1A''$ and the $2\,^1A'$ states are accessed, so the energy difference of ~0.17 eV between 223 and 230 nm photons causes a higher recoil velocity of the S and CO photofragments and possibly some higher rotational excitations for photolysis at 223 nm.

After the photolysis of OCS, the angular momentum of the CO($X\,^1\Sigma^+$) photofragment is oriented perpendicular to the plane of the O–C–S bending motion, which is a purely dynamical effect. The S cofragment, which is mainly released in the $^1D_2$ electronic state,[16] has an electronic angular momentum J which is also strongly polarized after the OCS photolysis.[19,23] This polarization, however, cannot be explained in terms of dynamics. For the bent OCS molecule, the $2\,^1A'$ excited state is accessed through a (nearly) parallel transition, whereas the $1\,^1A''$ state is accessed through a perpendicular transition. If in the excitation step both $2\,^1A'$ and $1\,^1A''$ states are accessed coherently, the dissociation proceeds on both energy surfaces, enabling the interference between the two dissociating pathways, as they lead to the same exit channel. If these two pathways differ energetically, this interference results in an asymptotic phase difference between the scattering wave functions, so measurement of the phase difference is a sensitive probe of the topology of the energy surfaces along the followed pathway.[10] Therefore, if the bending motion of the OCS parent molecule affects the pathway along which the molecule dissociates, the phase difference observed for $\nu_2=1$ and $\nu_2=0$ may not be the same. This phase difference is reflected in the photofragment angular momentum polarization as a $q=1$ contribution in the modified spherical harmonic formalism. The interference of simultaneously excited surfaces has been observed experimentally by measuring the $\mathrm{Im}[\mathbf{a}_1^{(1)}(\parallel,\perp)]$ orientation moment for OCS (Refs. 11 and 20) and iodine monochloride (ICl).[10] These measurements on the $\mathrm{Im}[\mathbf{a}_1^{(1)}(\parallel,\perp)]$ parameter,[11,20] as well as on other $\mathbf{a}_q^{(k)}(p)$ angular momentum polarization parameters,[12–15] are generally performed on non-state-selected parent molecules, so the observed parameters are averaged over several initial vibrational states of the parent molecule.

The effect of the parent molecule bending vibrational state ν_2 on the photolysis of OCS has been investigated experimentally before.[21,24,25] Observations of the orbital alignment and orientation of the S($^1D_2$) photofragment, however, have been reported for non-state-selected parent molecules only.[20,23] The orbital alignment of the O($^1D_2$) photofragment after the photolysis of the state-selected N_2O, which has a valence electron structure similar to OCS, has been reported by Teule *et al.*[26] Lee *et al.* very recently observed an orbital orientation in the photodissociation of ozone (O_3).[15]

In this paper we present state-to-state measurements on the photolysis of OCS at 223 and 230 nm for OCS in the rovibrational ground state $(\nu_1,\nu_2,\nu_3)=(0,0,0)$, denoted as $(\nu_2=0|JM=10)$, and in the first excited bending state $(\nu_1,\nu_2,\nu_3)=(0,1^1,0)$, denoted as $(\nu_2=1|J\ell M=111)$.[21] Using a hexapole state selector,[27] the effect of the parent molecule rovibrational state on the interference between the $2\,^1A'$ and $1\,^1A''$ dissociating pathways is investigated for the two mentioned dissociation wavelengths.

II. THEORY

The laboratory-frame spatial distribution of the dissociation products reflects the dynamical behavior of the molecule during the dissociation process and is commonly expressed in the anisotropy parameter β as

$$I(\theta_\epsilon)=\frac{\sigma}{4\pi}[1+\beta P_2(\cos\theta_\epsilon)], \tag{1}$$

where θ_ϵ is the laboratory-frame angle between the photolysis laser polarization and the recoil direction and P_2 the second-order Legendre polynomial. In the formalism in which the angular momentum polarization is expanded into spherical harmonics, as originally introduced by Kummel *et al.*[3] the corresponding coefficients, denoted as $A_q^{(k)}$, are not entirely independent from the laboratory frame. However, as shown by Rakitzis and Zare,[7] the photofragment-frame angular momentum polarization can be cast in a form in which the coefficients of the spherical harmonics in the photofragment frame are separated from the laboratory-frame variables, provided the value of β is known. In this formalism, the modified spherical harmonic coefficients are denoted as $\mathbf{a}_q^{(k)}(p)$, where the index p denotes whether the excitation to the dissociating energy surface is a purely parallel ($\parallel$), a purely perpendicular ($\perp$), or a mixed ($\parallel,\perp$) transition.[7]

The laboratory-frame detection probability of a polarized angular momentum distribution described by the $A_q^{(k)}$ polarization parameters, can also be expressed in terms of modified spherical harmonics:

$$I(\Theta,\Phi)=\sum_{k=0}^{2n}\sum_{q=-k}^{k}s_k A_q^{(k)} C_q^k(\Theta,\Phi), \tag{2}$$

where s_k is a parameter which depends on spectroscopic details of the transition to the resonant intermediate in case of a REMPI detection mechanism (as used in the experiments reported here), Θ is the polar angle between the recoil velocity and the probe-laser polarization, and Φ is the azimuthal angle between the pump and probe polarizations about the recoil velocity. As derived by Rakitzis,[28] and demonstrated experimentally,[23] several different pump-probe polarization geometries can be combined to obtain all angular momentum

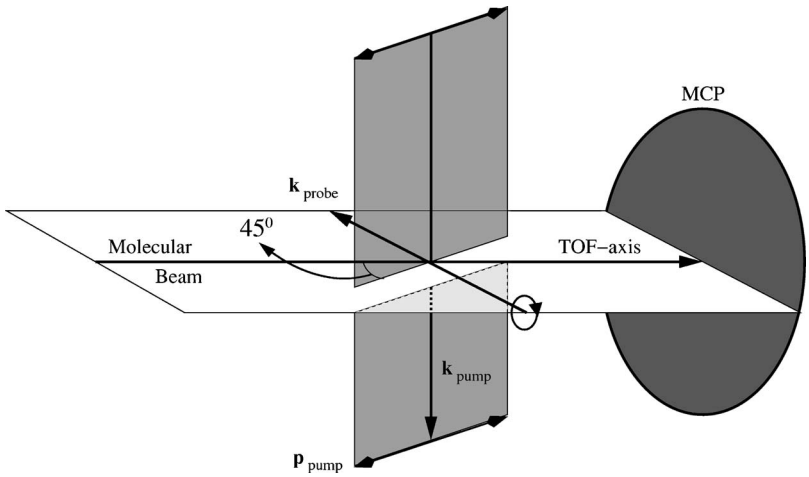

FIG. 1. Experimental geometry for detecting the $\mathrm{Im}\,\mathbf{a}_1^{(1)}(\parallel,\perp)$ interference parameter. The photolysis laser propagates top-down, and with its linear polarization $\mathbf{p}_{pump}$ at a 45° angle with the TOF axis. The plane of the photolysis laser polarization is indicated. The probe laser propagates horizontally and is circularly polarized.

polarization parameters. Furthermore, experimental conditions can be chosen such that the photofragment angular distribution becomes very sensitive to the $C_1^{(1)}$ orientation parameter.[11] This is the case in a pump-probe geometry in which the pump and probe lasers intersect under right angles, with the pump-laser linear polarization at an angle of 45° with respect to a circularly polarized probe-laser propagation direction (see Fig. 1). If all the ionized photofragments are detected simultaneously like in a velocity-map two-dimensional ion imaging detector, the three-dimensional (3D) distribution is projected onto the two-dimensional (2D) plane of the detector. For a monoenergetic 3D velocity distribution, the 2D projection of the $C_1^{(1)}$ term in the angular distribution, as observable in the geometry shown in Fig. 1, contributes to the data image as[11]

$$\frac{s_1\,\mathrm{Im}[\mathbf{a}_1^{(1)}(\parallel,\perp)]}{2\sqrt{2}}\frac{r^2\sin(2\theta')}{\sqrt{1-r^2}}, \tag{3}$$

where r and θ' are the cylindrical coordinates describing the 2D distribution as recorded by the detector and $\sin(2\theta')$ is the 2D-projected $C_1^{(1)}$ modified spherical harmonic. The angle θ' is measured relative to the direction of the polarization of the probe, $\theta'=0$ is in the direction of the propagation direction of the probe laser. The $q=1$ term may arise from the interference of scattering energy surfaces accessed through a mixed parallel *and* perpendicular transitions [i.e., $p=(\parallel,\perp)$].[5] The asymptotic phase difference $\Delta\phi$ is proportional to the observed $\mathrm{Im}[\mathbf{a}_1^{(1)}(\parallel,\perp)]$:

$$\mathrm{Im}[\mathbf{a}_1^{(1)}(\parallel,\perp)] \propto |\mu_\parallel||\mu_\perp|\sin(\Delta\phi). \tag{4}$$

This means that the $\mathrm{Im}[\mathbf{a}_1^{(1)}(\parallel,\perp)]$ parameter can only be nonzero if the β parameter is not equal to its limits +2 or −1. The boundary limits of β can be decreased by a nonzero angle between the asymptotic recoil direction and the transition dipole moment. The actual magnitude of the phase difference $\Delta\phi$ cannot be calculated from the $\mathrm{Im}[\mathbf{a}_1^{(1)}(\parallel,\perp)]$ parameter only, as the proportionality constant to $\sin\Delta\phi$ remains unknown, so only qualitative information can be extracted from $\mathrm{Im}[\mathbf{a}_1^{(1)}(\parallel,\perp)]$ measurements.

III. EXPERIMENT

The experimental setup has been described in detail before.[21,27] A 20% mixture of OCS in Ar is expanded through a nozzle and skimmed before it enters a buffer chamber which contains a beam stop, 20 cm downstream of the nozzle. This beam stop enhances the selectivity of the hexapole state selector which is positioned 10 cm downstream from the beam stop.[21] The molecules that pass the beam stop and which are in a positive Stark effect state are subsequently focused by the hexapole field onto a 1.5 mm collimator, located in the imaging chamber. By choosing the appropriate hexapole voltage,[21] either the $(\nu_2=0|JM=10)$ or the $(\nu_2=1|J\ell M=111)$ state is selected, utilizing the second- and first-order Stark effect, respectively.[29] The collimator is the entrance to the laser interaction region in the velocity-map electrostatic ion lens.[30] The state-selected molecular beam is intersected perpendicularly by a photolysis laser at a wavelength of 223 or 230 nm, which dissociates the OCS parent molecule into $\mathrm{CO}(X\,^1\Sigma^+)$ and $\mathrm{S}(^1D_2)$. Subsequently, both the photolysis laser and the molecular beam are intersected perpendicularly by a probe laser, which ionizes the nascent $\mathrm{S}(^1D_2)$ photofragments via a (2+1) REMPI scheme. For ionization through the $^1P_1$ and $^1F_3$ resonant intermediates, the probe laser is set at 291.39 and 288.11 nm (wavelengths in air), respectively. During data collection the probe laser was scanned over the Doppler profile of each atomic line. The S^+ ions are velocity mapped onto a position-sensitive detector [microchannel plate with a phosphor screen and charge-coupled device (CCD) camera]. The detector is positioned at the end of a 35 cm time-of-flight tube which is in line with the molecular-beam propagation direction. The microchannel plate (MCP) detector is gated in order to detect only the $\mathrm{S}(m/z=+32)$ ions. A CCD camera records the spatial intensity distribution of the light of the phosphor screen.

The $\mathrm{Im}[\mathbf{a}_1^{(1)}(\parallel,\perp)]$ parameter was measured by setting the linear polarization of the photolysis laser at an angle of 45° with respect to the propagation direction of the molecular beam. The probe laser is circularly polarized and ionizes the $\mathrm{S}(^1D_2)$ photofragments through the $^1P_1$ intermediate. A schematic picture of the applied experimental pump-probe geometry is given in Fig. 1.

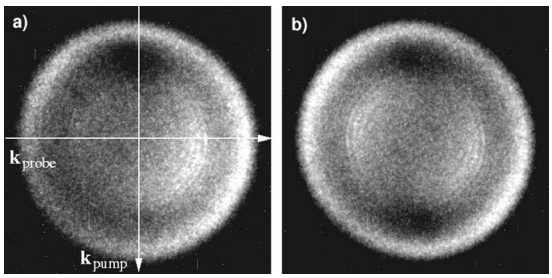

FIG. 2. (a) Raw data image of the 2D-projected recoil distribution of $S(^1D_2)$ after the OCS ($\nu_2=1|J\ell M=111$) photolysis at 230 nm. Both the pump and probe propagation directions are indicated. A left-right asymmetry due to parent molecule orientation is visible. (b) Sum image of the original data image in (a) and its inverted image. The effect of the parent molecule orientation, as observable in (a), has vanished. A remaining "tilt" in the image can be observed. This is caused by a $C_1^{(1)}$ contribution to the overall angular distribution.

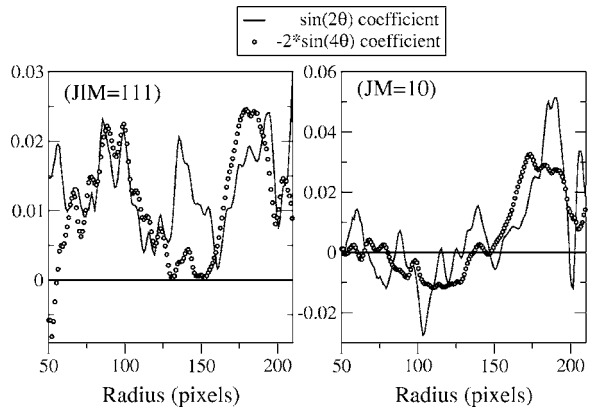

FIG. 3. Radial distribution of the $\sin(2\theta')$ and $\sin(4\theta')$ coefficients for the OCS ($\nu_2=1|J\ell M=111$) and ($\nu_2=0|JM=10$) photolysis at 230 nm and REMPI detection via the $^1F_3$ intermediate. The $\sin(4\theta')$ coefficient is multiplied by −2. Despite the very small amplitudes and the noisy signals, it can be seen that the $\sin(2\theta')$ amplitude is similar to $-2\cdot\sin 4\theta'$.

IV. RESULTS AND ANALYSIS

A typical data image of $S(^1D_2)$ following the photolysis of OCS ($\nu_2=1|J\ell M=111$) at 230 nm is shown in Fig. 2(a). First of all a very distinct left-right asymmetry is observed in the experimental data. As none of the atoms in the OCS molecule has a nuclear spin, the ($\nu_2=1|J\ell M=111$) state is almost completely oriented in the extraction field of the ion lens.[21] The orientation field is directed along the time-of-flight (TOF) axis which, in combination with a photolysis polarization at 45°, results in a left-right asymmetry in the angular distribution.[31] Recently, we utilized this asymmetry following from this photolysis geometry to study the photodissociation of spatially oriented OCS molecules, allowing the extraction of very detailed molecular-frame scattering information.[32,33] For the present study, however, the left-right asymmetry does not yield any additional information and is eliminated in the data to properly extract the $\mathrm{Im}[\mathbf{a}_1^{(1)}(\parallel,\perp)]$ parameter. The asymmetry is proportional to $\cos(\theta')$ in the 2D-projected image.[31] Since the 2D-projected $C_1^{(1)}(\Theta,\Phi)$ is proportional to $\sin(2\theta')$ and the projected even spherical harmonics ($k=0,2,4,\ldots$) are inversion symmetric, and $\cos(\theta')$ is not, we inverted the recorded data images about the center and added the inverted image to the original [see Fig. 2(b)]. This procedure eliminates the effect of the parent molecule orientation, as is clearly visible in the left-right symmetric image in Fig. 2(b).

In the symmetrized image in Fig. 2(b), we observe a very clear tilt in the intensity distribution away from 0° or 90°, especially for the fast outer channel. This tilt in the angular distribution is the result of the photofragment orbital orientation and is proportional to $\sin(2\theta')$, where θ' is the polar angle with respect to the pump-laser propagation vector ($\mathbf{k}_{\mathrm{pump}}$). For the outer channel, a stronger asymmetry is observed than for the inner channel.

Experimental geometries with the photolysis polarization at angles of +45° or −45° with respect to the molecular beam yield the same $\mathrm{Im}[\mathbf{a}_1^{(1)}(\parallel,\perp)]$ amplitude but of the opposite sign.[11] Therefore, subtracting the left-right symmetrized image measured at −45° photolysis polarization from the image taken at +45° yields $2\cdot\mathrm{Im}[\mathbf{a}_1^{(1)}(\parallel,\perp)]$. We used this procedure as we measured images at both +45° or −45°.

For the (2+1) REMPI transition via the $^1P_1$ intermedate, the line-strength factors $s_1=-5/\sqrt{6}$ and $s_3=0$.[3,4,34] However, for the ionization via the $^1F_3$ intermediate, $s_1=0$ and $s_3=-5/7\sqrt{3/2}$. Although the $C_1^{(1)}(\Theta,\Phi)$ and $C_1^{(3)}(\Theta,\Phi)$ modified spherical harmonics are orthogonal, their 2D projections are not. The 2D $C_1^{(1)}(\Theta,\Phi)$ projection is proportional to $\sin(2\theta')$, whereas the $C_1^{(3)}(\Theta,\Phi)$ projection is proportional to $[\sin(4\theta')-2\sin(2\theta')]$. Consequently, a nonzero $C_1^{(3)}(\Theta,\Phi)$ term in the 3D recoil distribution implies a $C_1^{(1)}(\Theta,\Phi)$ contribution to the 2D projected data. As all $C_{q=1}^k$ terms result from the same quantum interference effect,[7] the recoil distribution of $S(^1D_2)$ detected via the $^1F_3$ intermediate must contain a $C_1^{(3)}(\Theta,\Phi)$ contribution. Therefore, in the angular distribution of the 2D data images following a REMPI detection via the $^1F_3$ intermediate, a $\sin(4\theta')$ term must be observable, as well as an $\mathrm{Im}[\mathbf{a}_1^{(1)}]$ term, which must have the magnitude of $-2\cdot\sin(4\theta')$. As shown in Fig. 3, this proportionality between the $\sin(2\theta')$ and $\sin(4\theta')$ amplitudes is generally observed after subtracting the −45° data from the +45° data. This demonstrates that subtracting the −45° from the +45° data is internally consistent and properly isolates the contributions for the $\mathrm{Im}[\mathbf{a}_1^{(1)}]$ parameter. For all the results presented here we used the $S(^1P_1)$ state as the intermediate level in the (2+1) REMPI ionization of $S(^1D_2)$.

The magnitude of $\mathrm{Im}[\mathbf{a}_1^{(1)}]$ (solid line) and the velocity distribution (dashed line) following 230 nm photolysis of OCS ($\nu_2=1|J\ell M=111$) and ($\nu_2=0|JM=10$) are plotted in Figs. 4(a) and 4(b), respectively. In Figs. 5(a) and 5(b), the distributions are shown for photolysis at 223 nm. In Figs. 4 and 5, the angular distribution at small radii (i.e., small velocities) was not calculated. When analyzing the angular distribution of a radial slice $r\cdots(r+\Delta r)$, the pixels within the range $r\cdots(r+\Delta r)$ are divided over a fixed number of angular bins (20 in our case). As the number of bins is the same for each evaluated radial slice, there were too few pixels in the slice to fill each bin at small radii. Therefore, the angular distribution at small radii is not presented. Also at large velocities ($v>1100$ m/s) the intensity was too low to give meaningful results.

One of the initial motivations of the experiment was to

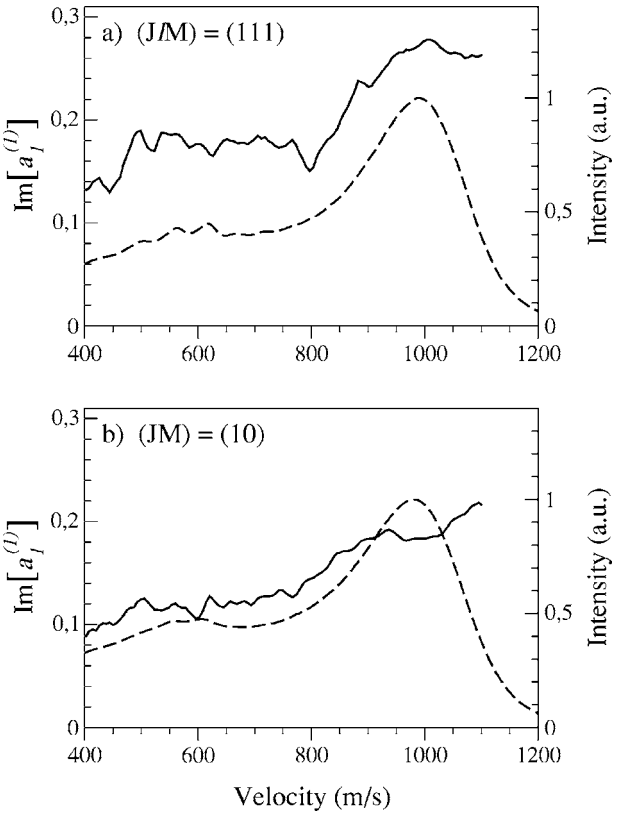

FIG. 4. (a) Magnitude of Im[$\mathbf{a}_1^{(1)}$] (solid line) as a function of velocity of S($^1D_2$) after the OCS ($\nu_2=1|J\ell M=111$) photolysis at 230 nm and probing of S($^1D_2$) via the $^1P_1$ intermediate. The velocity distribution is also shown (dashed line). (b) Same as (a) but for the OCS ($\nu_2=0|JM=10$) initial state. The Im[$\mathbf{a}_1^{(1)}$] curves are obtained by subtracting the data recorded at −45° from the data obtained at +45°. The Im[$\mathbf{a}_1^{(1)}$] amplitude is obtained from the fitted sin($2\theta'$) coefficient, as follows from Eq. (3).

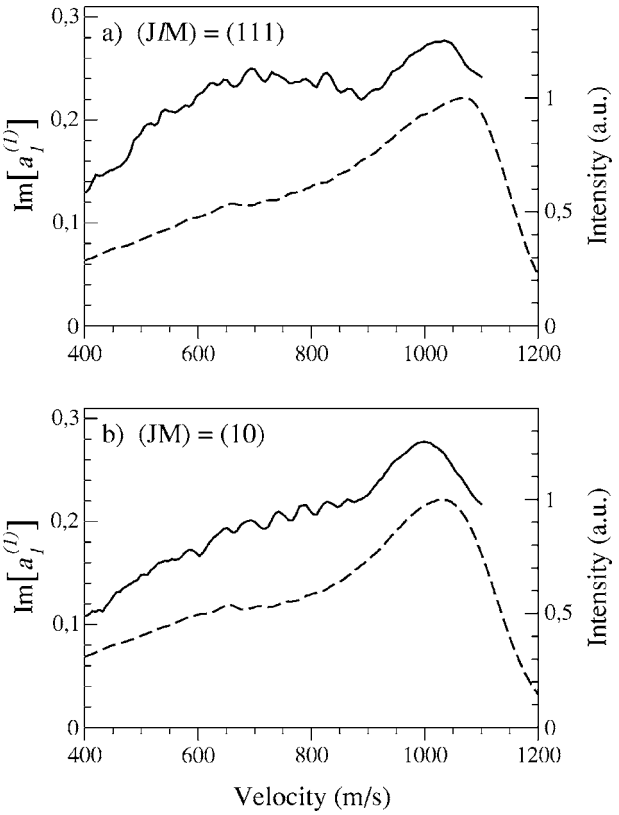

FIG. 5. (a) Magnitude of Im[$\mathbf{a}_1^{(1)}$] (solid line) as a function of velocity of S($^1D_2$) after the OCS ($\nu_2=1|J\ell M=111$) photolysis at 223 nm and probing of S($^1D_2$) via the $^1P_1$ intermediate. The velocity distribution is also shown (dashed line). (b) Same as (a) but for the OCS ($\nu_2=0|JM=10$) initial state.

employ various pump-probe geometries to obtain all $\mathbf{a}_q^{(k)}(p)$ parameters of the S($^1D_2$) photofragment following the OCS ($J\ell M|\nu_2$) photolysis at 223 and 230 nm, like what was demonstrated for the non-state-selected OCS by Rakitzis *et al.*[23] In these detection geometries the pump and probe lasers intersect perpendicularly and while the pump laser is linearly polarized, the probe laser is circularly polarized [linear-circular (LC) geometry] or vice versa [circular-linear (CL) geometry]. The 3D spatial distribution of the ionized S($^1D_2$) photofragments is cylindrically symmetric so the recorded data images are Abel invertible. We analyzed this data extensively but we obtained little new information, and therefore we do not report this data here. However, the velocity distributions appeared more meaningful. Data images of S($^1D_2$) after the OCS ($\nu_2=0|JM=10$) photolysis at 230 nm, detected via the $^1P_1$ resonant intermediate and measured in the LC and CL geometries, are shown in Figs. 6(a) and 6(b), respectively. The fast and slow channels are clearly distinguishable, and for the fast channel the LC and CL geometries yield strongly different angular distributions. The CO(J) rotational structure is visible as individual rings in the slow channel. This is even more obvious in the velocity distributions, obtained from the Abel-inverted data images, which are plotted in Fig. 7 for photolysis at 223 and 230 nm. A small shift to a higher velocity for the 223 nm photolysis with respect to the 230 nm photolysis is observed, indicating that a large fraction of the additional photon energy (~75% at the peak of the fast channel of the velocity distribution) is channeled into rotational motion. The most intense rotational lines in the slow channel are indicated. The lines were assigned using an OC–S bond energy D_0 of 4.292 eV. Note that the bond energy D_0 of 4.292 eV is a correction of the value of 4.284 eV, which has been published before.[21] An OCS bending energy of 520 cm^{-1} (Ref. 35) and CO(J) rotational energies of 7892.87 and 9144.09 cm^{-1} for $J=64$ and 69 were used, respectively.[22] Furthermore, the slow channel

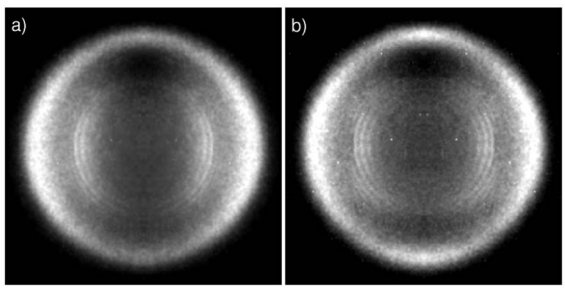

FIG. 6. (a) Raw data image of the 2D-projected recoil distribution of S($^1D_2$) after the OCS ($\nu_2=0|JM=10$) photolysis at 230 nm recorded in the LC geometry, where the photolysis laser propagates top-down, with its linear polarization in the plane of the image, and the circularly polarized probe laser propagates left-right. The S($^1D_2$) atom was ionized via the $^1P_1$ intermediate. (b) Same as (a) but recorded in the CL geometry, where the photolysis laser is circularly polarized and the probe laser is linearly polarized, with its polarization axis in the plane of the image.

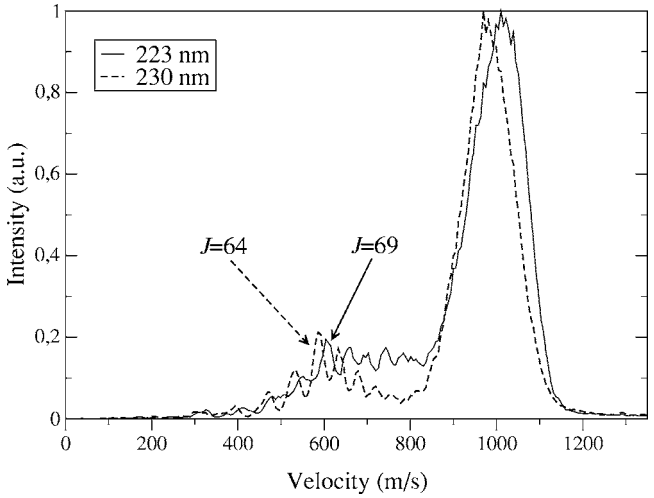

FIG. 7. Velocity distributions of the $S(^1D_2)$ photofragments after the OCS $(\nu_2=1|J\ell M=111)$, detected in the LC geometry via the $^1P_1$ intermediate. For the photolysis at both 223 nm (solid line) and 230 nm (dashed line), the CO(*J*) rotational structure is visible in the $S(^1D_2)$ velocity distribution. The most intense rotational lines in the slow channel are indicated.

is more populated for the 223 nm photolysis than for the 230 nm photolysis, in agreement with observations by Suzuki *et al.*[19]

V. DISCUSSION

In the measurements reported here we photolyze single-quantum state-selected parent OCS molecules. For the fast $S(^1D_2)$ channel from the photolysis at 230 nm, an increasing $\mathrm{Im}[\mathbf{a}_1^{(1)}]$ moment with increasing OCS bending motion is observed. At the peak of the velocity distribution (see Fig. 4) $\mathrm{Im}[\mathbf{a}_1^{(1)}]=0.28$ for the dissociation of vibrationally excited OCS, whereas for the photolysis of ground-state OCS $\mathrm{Im}[\mathbf{a}_1^{(1)}]$ drops to 0.18. At the 223 nm photolysis the $\mathrm{Im}[\mathbf{a}_1^{(1)}]$ moment for fast $S(^1D_2)$ is very much similar for vibrationally excited and ground-state OCS.

In the past there have been two studies reporting the measurement of $\mathrm{Im}[\mathbf{a}_1^{(1)}]$ for the photodissociation of non-state-selected OCS molecules. Both the measurement by Kim *et al.*[20] at the 223 nm photolysis and the experiment by Rakitzis *et al.*[11] at the 230 nm photolysis were done in a non-state-selected molecular beam. The energy spacing between the vibrational ground state and the first-excited doubly degenerate $\nu_2=1$ vibrational state equals 520.4 cm^{-1},[35] so at room temperature about 14% of the OCS sample is in the $\nu_2=1$ state. *Ab initio* calculations by Suzuki *et al.*[19] show that the absorption cross section for OCS molecules in the first-excited bending state is larger than for OCS in the vibrational ground state. This means that the fraction of OCS molecules in the excited bending state that is dissociated is effectively (much) more than 14%, even as the vibrational cooling in the expansion of the molecular beam will reduce the vibrationally excited fraction relative to the fraction at room temperature.

To compare our results with the averaged data reported before on the fast and slow channels we calculated the weighted average of the $\mathrm{Im}[\mathbf{a}_1^{(1)}]$ over the velocity distribution. The averaged $\mathrm{Im}[\mathbf{a}_1^{(1)}]$ values are given in Table I, for both the $(\nu_2=1|J\ell M=111)$ and the $(\nu_2=0|JM=10)$ parent molecule states and photolysis at 230 and 223 nm. For the photolysis at 230 nm of ground-state molecules, $(\nu_2=0|JM=10)$, the value of the averaged $\mathrm{Im}[\mathbf{a}_1^{(1)}]$ moment for the fast channel, 0.19, is comparable with observations by Rakitzis *et al.*,[11] where the OCS molecules were not state selected. The state selection of the OCS $(\nu_2=0|JM=10)$ parent molecule in our experiment is not entirely pure.[21] Therefore, the observed values for the dissociation of OCS $(\nu_2=0|JM=10)$ contain a contribution from the dissociation of the $(\nu_2=1|J\ell M=111)$ state. As the $\mathrm{Im}[\mathbf{a}_1^{(1)}]$ values for the $(\nu_2=1|J\ell M=111)$ state are higher than those of the $(\nu_2=0|JM=10)$ state, the real values for the $(\nu_2=0|JM=10)$ are expected to be even somewhat lower than what we observed experimentally.

TABLE I. Weighted average of the fast- and slow-channel $\mathrm{Im}[\mathbf{a}_1^{(1)}]$ values for both initial parent molecule states and both 230 and 223 nm photolysis wavelengths. For the 230 nm photolysis, the fast and slow channels are defined as the velocity ranges 759–1167 and 245–753 m/s, respectively. For the 223 nm photolysis they are defined as 852–1196 and 291–846 m/s, respectively. Note that the magnitude of $\mathrm{Im}[\mathbf{a}1(1)]$ for the slow channel is affected by a large contribution from the fast channel and the value should be taken with caution.

	230 nm photolysis		223 nm photolysis	
	fast channel	slow channel	fast channel	slow channel
$(\nu_2=1\|J\ell M=111)$	0.25	0.16	0.25	0.21
$(\nu_2=0\|JM=10)$	0.19	0.11	0.24	0.18

For the photolysis at 223 nm, we observe only a very small difference in the $\mathrm{Im}[\mathbf{a}_1^{(1)}]$ amplitude between the slow and the fast channels (see Fig. 5 and Table I). Kim *et al.*[20] reported, for the OCS photolysis at 223 nm, a comparable amplitude for the fast channel (~0.25) but a considerably lower value for the slow channel (~0.03). In our experiments, the geometry of the setup is not cylindrically symmetric and no Abel inversion can be applied. We extract the angular distributions directly from the 2D projected spatial distribution. As can be seen in Eq. (3), the 2D projection of the original 3D distribution of each rotational line gives a contribution to the $\mathrm{Im}[\mathbf{a}_1^{(1)}]$ amplitude at lower radii. The $\mathrm{Im}[\mathbf{a}_1^{(1)}]$ values observed by Kim *et al.*[20] were obtained by extracting the core of the spatial distribution of $S(^1D_2)$ photofragments, so in their experiments the original recoil distribution was retained and the slow channel $\mathrm{Im}[\mathbf{a}_1^{(1)}]$ values have no contribution from the fast channel. Equations (8), (9), and (11) from Ref. 31 can be used to simulate how the 3D recoil distribution is projected onto a 2D plane. The fast and slow channels are approximated by Gaussian functions of which the centers and full-width-at-half-maximum (FWHM) magnitudes are estimated from the velocity distribution displayed in Fig. 7. The contribution of the fast-channel to the slow-channel signal intensity is estimated to be up to 80%, which accounts for the high $\mathrm{Im}[\mathbf{a}_1^{(1)}]$ observed for the slow channels in all our data images. This means that the extracted values for the slow channel reported here are higher than they are in reality. Recently, a new version of velocity-map imaging, called slice imaging, was

developed[36,37] where a fast gate on the MCP detector slices a narrow part of the 3D distribution. Using slice imaging instead of velocity mapping, the $\mathrm{Im}[\mathbf{a}_1^{(1)}]$ amplitudes of the fast and slow channels can be separated experimentally. We plan on doing such slice imaging experiments in the future.

As follows from Eq. (4), the $\mathrm{Im}[\mathbf{a}_1^{(1)}]$ amplitude is proportional to the product of the transition dipole moments of the excitations to the individual $2\,^1A'$ and $1\,^1A''$ energy surfaces. The β parameters can be used to estimate the contributions of the parallel and perpendicular transitions. The β values for dissociation of both initial rovibrational states of OCS states have been reported elsewhere for the 230 nm photolysis.[21] For the fast channel, which follows from the coherent excitation by a 230 nm photon, the fraction $f_\parallel$ of the $2\,^1A'$ excitation decreases from 0.61 for the $(\nu_2=1|J\ell M=111)$ state to 0.44 for the $(\nu_2=0|JM=10)$ state. Here it is taken into account that the β value for the pure parallel transition equals ~ 1.8.[21] The product of the transition dipole moments, however, does not change as $\sqrt{0.61\times(1-0.61)} \approx \sqrt{0.44\times(1-0.44)}$, so no significant difference in the $\mathrm{Im}[\mathbf{a}_1^{(1)}]$ value should be expected between both parent molecule bending modes. Nevertheless, we observe an increase from 0.18 to 0.28 for the dissociation of the linear versus the bent OCS molecule.

In a very recent paper, Lee *et al.* measured the orientation in the $\mathrm{O}(^1D_2)$ photofragments from the photodissociation of ozone with a linearly polarized light.[15] More remarkably, this orientation (described by the $\mathrm{Im}[\mathbf{a}_1^{(1)}]$ parameter, or the γ_1' parameter using an alternative formalism[6]) was produced from the excitation to a single electronic state. Furthermore, the photofragment orientation of $\mathrm{O}(^1D_2)$ changed as a function of recoil speed.[15] At first this seems at odds with the interpretation of the $\mathrm{Im}[\mathbf{a}_1^{(1)}]$ parameter as an interference term between the excitation to states via parallel and perpendicular transitions. However, the symmetry of the excited state in the highly bent ozone molecule is neither parallel nor perpendicular to the recoil direction, but possesses a large angle between the transition dipole moment and the recoil direction. Vasyutinskii and co-workers postulate that a phase difference between the parallel and perpendicular components is introduced and modulated by angle-dependent long-range interactions. We consider whether a similar mechanism can be acting in OCS. In principle, these two mechanisms, single-surface versus two-surface dynamics, leading to coherences in the polarization have different dynamical origins. The transition dipole moment of the A'' state is purely perpendicular to the recoil direction, so it cannot produce a "single-surface" contribution to the $\mathrm{Im}[\mathbf{a}_1^{(1)}]$. The transition dipole of the A' surface does have a small angle (about 13°) to the recoil direction,[21,32] so it can, in principle, have a "single-surface" contribution to the $\mathrm{Im}[\mathbf{a}_1^{(1)}]$. However, because of this small angle we expect such a contribution to be much smaller than in the case of ozone. The observed $\mathrm{Im}[\mathbf{a}_1^{(1)}]$ is largest when there is an approximately equal contribution to the excitation by the A' and A'' states and decreases as these contributions become unequal, as expected for the interference between these states.

To the best of our knowledge no values for β have been reported for the individual OCS $(\nu_2=0|JM=10)$ and $(\nu_2=1|J\ell M=111)$ rovibrational states for photodissociation at 223 nm. Suzuki *et al.* reported a value of 0.7 for β only for non-state-selected molecules.[19] The photodissociation process at 223 nm is probably not much different from 230 nm, and the product of transition dipole moments is not very sensitive at $\beta \approx 0.7$, so this product for each of the rovibronic states will not be much different from that observed at 230 nm. The interpretation of the observed $\mathrm{Im}[\mathbf{a}_1^{(1)}]$ parameters at 223 nm remains open for debate. It is obvious, however, that the observed $\mathrm{Im}[\mathbf{a}_1^{(1)}]$ for OCS in the $(\nu_2=0|JM=10)$ state does depend on the wavelength, so the followed pathway on the PES is probably affected by the photon energy.

In conclusion, although some single-surface contribution to the $\mathrm{Im}[\mathbf{a}_1^{(1)}]$ moment cannot be ruled out, we believe that the main contribution to the $\mathrm{Im}[\mathbf{a}_1^{(1)}]$ moment is due to a phase shift between at least two surfaces. The differences of the $\mathrm{Im}[\mathbf{a}_1^{(1)}]$ moment as a function of initial state or photolysis energy show a variation in the phase shift or amplitudes from the contributing states. We infer that at the 230 nm photolysis the bent molecule follows a somewhat different pathway on the dissociating surfaces than the linear molecule, leading to a different phase difference $\Delta\phi$. It would be highly desirable to compare our results with quantum calculations on high-level *ab initio* surfaces, which seem at the moment quite challenging and are not available yet.

Energy conservation causes the rotational excitation of the $\mathrm{CO}(J)$ photofragment to be correlated and reflected in the kinetic-energy distribution of the $\mathrm{S}(^1D_2)$ cofragment. This is most clearly demonstrated by the rotational structure we observe in the slow channel of the velocity distribution (Fig. 7). Nishide and Suzuki recently observed a N_2 rotational structure in the $\mathrm{O}(^1D_2)$ velocity distribution for the N_2O photolysis around 203–205 nm.[38] N_2O has an electronic structure very similar to that of OCS. Nishide and Suzuki used a molecular beam optimized for vibrational cooling of the parent molecules, a more refined velocity-mapping ion lens and a very high resolution imaging detector. In our experiments we use state-selected parent molecules, which limits the degrees of freedom to a minimum and thereby enhances the resolution of the recoil distribution. Furthermore, the focused laser beams intersect each other perpendicularly, which gives a very small detection volume in the electrostatic lens, which enhances the resolution even further. Notwithstanding the lower resolution of the imaging detector in our setup, the experimental conditions were sufficient to observe an obvious $\mathrm{CO}(J)$ rotational structure even in the raw, non-Abel-inverted data images recorded for detecting the $\mathrm{Im}[\mathbf{a}_1^{(1)}]$ parameter (Fig. 2) as well as in the LC and CL geometries [Figs. 6(a) and 6(b), respectively]. Although not shown here, in the data images taken in the LC and CL geometries with REMPI detection via the $^1F_3$ intermediate, the $\mathrm{CO}(J)$ rotational structure was observed as well.

VI. CONCLUSIONS

By measuring the $\mathrm{Im}[\mathbf{a}_1^{(1)}]$ moment in the angular momentum polarization of the $\mathrm{S}(^1D_2)$ photofragment we inves-

tigated whether the photolysis wavelength and the parent molecule rovibrational state have an effect on how the potential-energy surfaces are sampled during the photolysis of OCS. The OCS parent molecules were prepared in either the $(\nu_2=0|JM=10)$ or the $(\nu_2=1|J\ell M=111)$ rovibrational state, and the dissociation wavelengths used were 223 and 230 nm. At the 230 nm photolysis the OCS rovibrational state is found to affect the followed pathway; an increase of about 50% in the $\mathrm{Im}[\mathbf{a}_1^{(1)}]$ moment is observed. However, for the photolysis at 223 nm the observed $\mathrm{Im}[\mathbf{a}_1^{(1)}(\parallel,\perp)]$ parameter does not change with the initial OCS state. The experimental data suggest that the photolysis wavelength does affect the pathway for OCS in the $(\nu_2=0|JM=10)$ rovibrational ground state.

The CO(J) rotational structure is clearly observed for the slow S($^1D_2$) channel in the velocity spectra extracted from the Abel-inverted images. From the velocity spectra we conclude that the majority ($\sim$75%) of the additional photon energy, $\sim$1365 cm^{-1} when changing from 230 to 223 nm photolysis wavelengths is channeled into the rotational rather than the translational motion. An improved value for the OC–S bond energy $D_0=4.292$ eV is reported.

ACKNOWLEDGMENTS

This research has been financially supported by the councils for Chemical Sciences and Physical Sciences of the Dutch Organization for Scientific Research (NWO-CW, NWO-FOM). A.J.v.d.B. thanks the EU for the support as a Marie Curie Training Institute fellow at IESL-FORTH under Contract No. HPMT-CT-2000-00201. T.P.R. thanks the EU for the support to access the experimental facilities of the Laser Center Vrije Universiteit through the EU program HPRI-CT-1999-00064. M.H.M.J. thanks the Community's Human Potential Program under Contract No. HPRN-CT-1999-00129 (COCOMO) for the support at FORTH.

[1] U. Fano and J. H. Macek, Rev. Mod. Phys. **45**, 553 (1973).
[2] C. H. Greene and R. N. Zare, J. Chem. Phys. **78**, 6741 (1983).
[3] A. C. Kummel, G. O. Sitz, and R. N. Zare, J. Chem. Phys. **85**, 6874 (1986).
[4] A. C. Kummel, G. O. Sitz, and R. N. Zare, J. Chem. Phys. **88**, 6707 (1988).
[5] L. D. A. Siebbeles, M. Glass-Maujean, O. S. Vasyutinskii, J. A. Beswick, and R. Octavio, J. Chem. Phys. **100**, 3610 (1994).
[6] A. S. Bracker, E. R. Wouters, A. G. Suits, and O. S. Vasyutinskii, J. Chem. Phys. **110**, 6749 (1999).
[7] T. P. Rakitzis and R. N. Zare, J. Chem. Phys. **110**, 3341 (1999).
[8] A. Brown, G. G. Balint-Kurti, and O. S. Vasyutinskii, J. Phys. Chem. A **108**, 7790 (2004).
[9] A. Smolin, O. S. Vasyutinskii, E. Wouters, and A. Suits, J. Chem. Phys. **121**, 6759 (2004).
[10] T. P. Rakitzis, S. A. Kandel, A. J. Alexander, Z. H. Kim, and R. N. Zare, Science **281**, 1346 (1998).
[11] T. P. Rakitzis, P. C. Samartzis, and T. N. Kitsopoulos, J. Chem. Phys. **111**, 10415 (1999).
[12] M. Ahmed, E. R. Wouters, D. S. Peterka, O. S. Vasyutinskii, and A. G. Suits, Faraday Discuss. **113**, 425 (1999).
[13] E. R. Wouters, M. Beckert, L. J. Russel, K. N. Rosser, A. J. Orr-Ewing, M. R. N. Ashfold, and O. S. Vasyutinskii, J. Chem. Phys. **117**, 2087 (2002).
[14] M. Brouard, R. Cireasa, A. P. Clark, C. Vallence, G. Groenenboom, and O. S. Vasyutinskii, J. Phys. Chem. A **108**, 7965 (2004).
[15] S. K. Lee, D. Townsend, O. S. Vasyutinskii, and A. G. Suits, Phys. Chem. Chem. Phys. **7**, 1650 (2005).
[16] G. Nan, I. Burak, and P. L. Houston, Chem. Phys. Lett. **209**, 383 (1993).
[17] N. Sivakumar, G. E. Hall, P. L. Houston, J. W. Hepburn, and I. Burak, J. Chem. Phys. **88**, 3692 (1988).
[18] Y. Sato, Y. Matsumi, M. Kawasaki, K. Tsukiyama, and R. Bersohn, J. Phys. Chem. **99**, 16307 (1995).
[19] T. Suzuki, H. Katayanagi, S. Nanbu, and M. Aoyagi, J. Chem. Phys. **109**, 5778 (1998).
[20] Z. H. Kim, A. J. Alexander, and R. N. Zare, J. Phys. Chem. A **103**, 10144 (1999).
[21] A. J. van den Brom, T. P. Rakitzis, J. van Heyst, T. N. Kitsopoulos, S. R. Jezowski, and M. H. M. Janssen, J. Chem. Phys. **117**, 4255 (2002).
[22] A. M. Rijs, E. H. G. Backus, C. A. de Lange, M. H. M. Janssen, N. P. C. Westwood, K. Wang, and V. McKoy, J. Chem. Phys. **116**, 2776 (2002).
[23] T. P. Rakitzis, P. C. Samartzis, and T. N. Kitsopoulos, Phys. Rev. Lett. **87**, 123001 (2001).
[24] A. Sugita, M. Mashino, M. Kawasaki, Y. Matsumi, R. Bersohn, G. Trott-Kriegeskort, and K.-H. Gericke, J. Chem. Phys. **112**, 7095 (2000).
[25] H. Katayanagi and T. Suzuki, Chem. Phys. Lett. **360**, 104 (2002).
[26] J. M. Teule, G. C. Groenenboom, D. W. Neyer, D. W. Chandler, and M. H. M. Janssen, Chem. Phys. Lett. **320**, 177 (2000).
[27] M. H. M. Janssen, J. W. G. Mastenbroek, and S. Stolte, J. Phys. Chem. A **101**, 7605 (1997).
[28] T. P. Rakitzis, Chem. Phys. Lett. **342**, 121 (2001).
[29] S. R. Ghandi and R. N. Bernstein, J. Chem. Phys. **87**, 6457 (1987).
[30] A. T. J. B. Eppink and D. H. Parker, Rev. Sci. Instrum. **68**, 3477 (1997).
[31] T. P. Rakitzis, A. J. van den Brom, and M. H. M. Janssen, Chem. Phys. Lett. **372**, 187 (2003).
[32] T. P. Rakitzis, A. J. van den Brom, and M. H. M. Janssen, Science **303**, 1852 (2004).
[33] A. J. van den Brom, T. P. Rakitzis, and M. H. M. Janssen, J. Chem. Phys. **121**, 11645 (2004).
[34] T. P. Rakitzis, S. A. Kandel, and R. N. Zare, J. Chem. Phys. **22**, 9382 (1997).
[35] Y. Morino and T. Nakagawa, J. Mol. Spectrosc. **26**, 496 (1968).
[36] C. R. Gebhardt, T. P. Rakitzis, P. C. Samartzis, V. Ladopoulos, and T. N. Kitsopoulos, Rev. Sci. Instrum. **72**, 3848 (2001).
[37] D. Townsend, M. Minitti, and A. G. Suits, Rev. Sci. Instrum. **74**, 2530 (2003).
[38] T. Nishide and T. Suzuki, J. Phys. Chem. A **108**, 7863 (2004).